THE COMPUTATION AND VALIDATION OF HOVERING ROTOR PERFORMANCE

M. Nsi Mba
Institut Mecanique de Marseille
Marseilles, France

K. Ramachandran
Flow Analysis Inc.
Ames Research Center

F. X. Caradonna
Aeroflightdynamics Directorate
U. S. Army Aviation Systems Command (AVSCOM)
Ames Research Center
Moffett Field, California

INTRODUCTION

The prediction of helicopter hover performance is a demanding problem - both because of the physical/computational difficulty of the problem as well as the importance of the problem to the design of helicopters. The physical difficulty arises because the hovering rotor must operate in close proximity to its' own wake (Fig. 1). The structure and location of this wake is the single most important element determining the performance of the rotor and all treatments of the hover problem must center on this wake prediction. The classical computational problem is that free wakes are physically unstable. The acute sensitivity of the problem to an unstable wake is the root of many difficulties seen in hover computations.

Presented at the 17th European Rotorcraft Forum, Berlin, Germany, September 24-27, 1991

The flow near the rotor blade surface itself is also an important determinant of performance. None of the classical integral free wake codes can predict this compressible, 3-dimensional flow. However, the typical rotor blade is a high aspect ratio rectangular configuration, which rarely encounters significant separation. Therefore, the use of empirical airfoil tables, (to give lift and/or profile drag) derived from 2-D testing, has been considered adequate in the past. Testing has also been a primary means of circumventing the free-wake instability problem. That is, rotor inflow computations are most often obtained with the aid of prescribed wake geometry data obtained from model rotor flow visualization tests (Ref. 1 and 2). Thus the current mainstays of engineering hover analyses require empirical data to obtain both the induced and the profile power.

However, an optimum rotor need not be the traditional configuration for which existing empiricisms are designed. There is, therefore, a need for analysis schemes which are

much less dependent on test data. The search for such schemes (especially free-wake methods) has a long history and is far from complete.

The oldest form of rotor computational methods are boundary integral methods applied to predicting the wake (and the related inflow) of hovering rotors. The long history of such methods is testimony both to the importance of the hover free-wake problem and to its' difficulty. The use of boundary integral methods (usually methods in which wakes are modeled by a sparse vortex lattice) has been dictated by the engineering need for computational efficiency and enabled by the fact that the wake flow is essentially incompressible. However, the rotor flow itself is far from incompressible. To account for compressibility and other effects not encompassed in this theory, these methods have often described the rotor by a lifting line (or a sparse lifting surface) with compressible real gas effects being handled by the use of tabular airfoil data - often combined with empirical tip corrections. To date, several impressive hover studies have been performed using these methods. The recent papers of Felker et al (Ref. 3) and Shanley et al (Ref. 4), both of which use the vortex lattice method of Bliss and Quackenbush (Ref. 5), are notable recent examples.

The use of Computational Fluid Dynamics (CFD) is new to this problem. Traditionally, the term CFD refers to the use of differential (finite difference, finite volume, finite element) methods in which the entire flowfield is solved for. The traditional CFD methods (potential, Euler and Navier-Stokes) are mainly suited to solving for the flows close to the rotor surface because they use fixed grids, which cannot easily convect flow quantities (such as circulation) without excessive numerical dissipation. Therefore, the obvious utility of these methods is to obviate the need for airfoil empirical data (except for cases involving massive separation). In recent years, classical CFD methods have also attained some success in treating the hover wake problem using low dissipation algorithms and the careful use of dense grids (Ref. 6,7 and 8). The recent paper of Srinivasan et al (Ref. 8) is notable in this respect.

The big advantage of the boundary-integral methods is that they are Lagrangian: they physically track individual wake elements and are not subject to dissipation. However, CFD methods can also employ Lagrangian tracking concepts. The first of these to be used for rotors is the vortex embedding scheme of Ramachandran and Steinhoff (Ref. 9 and 10). In this method, trailed rotor circulation elements are physically tracked and then embedded into a conventional full-potential CFD code by means of a Clebsch kinematical description of the flow. This method has been incorporated into a code called "HELIX-I".

Because, the latter approach is the first which can dispense with both wake and profile empiricisms, it has become an object of joint study by the U.S. Army Aeroflightdynamics Directorate (AFDD) and the Institut de Mecanique des Fluides Marseille (IMFM) under the the auspices of the U.S./France

MOU for rotor dynamics. This study is centered on a base of model rotor hover data, obtained by IMFM (Ref. 11 and 12) and Aerospatiale Helicopters (Ref. 13). This data base includes extensive measurements on many rotor configurations. Using these data as a basis of study, this report is aimed at presenting some of our recent experience with the HELIX-I code and its ability to predict the flow and performance of both conventional rotors and the unconventional, anhedral parabolic tip rotor used on the Super Puma MK2.

EXPERIMENTAL ROTOR STUDIES

Most of the hover data used in this work was obtained in the IMFM 3.3 x 2.2 m wind tunnel located in Marseilles. This is a low speed, open-circuit, tunnel with an elliptic cross section and an open test section. The rotors were mounted on a very versatile stand (Fig. 2), which permits the operation of model rotors in both the axial or edge-wise flight mode. For the present data, the model rotors were mounted such that the rotor and tunnel axes were parallel to each other. The open test section permitted the operation of fairly large rotors (1.5 m diameter) - relative to the test section - with no noticeable tunnel wall effects.

In addition to the usual performance data, extensive flow-field diagnostic data was also obtained at IMFM. The tip vortex trajectories were measured using a traversing hot wire probe. Tip-vortex trajectory data were also obtained by smoke flow-visualization techniques.

Direct measurements were also made of the velocity field of the rotor, using a two-component laser velocimeter (Fig. 3). In addition to obtaining extensive velocity distributions both above and below the rotor, these data were also used to make measurements of the rotor radial circulation distribution. To obtain this circulation at any blade radius, the LV (laser velocimeter) data acquisition is timed and positioned to obtain velocity data that is appropriate for computing a line integral about the blade. Ideally, this line integral should be made as close as possible to the blade. However, equipment limitations have prevented the acquisition of such data just ahead or behind the blade. Therefore, a circulation integration procedure was developed, in which the line integral extends fully from one blade to the next (Fig. 4). This obviated the need to include the vertical components of the line integrals (because of cancellation due to flow periodicity), and is a much simplified procedure.

For more detailed information on these test procedures, the reader is referred to Ref. 11 and 12. Model Super Puma data and the rigs used for obtaining it are described in Ref. 13 and 14, respectively.

THE COMPUTATIONAL METHOD

The present computational method is based on solving the steady mass conservation equation,

$$\nabla \cdot (\rho \vec{V}) = 0 \qquad (1)$$

We assume that the density, ρ, (normalized by free-stream value) takes the usual isentropic form,

$$\rho = \left[1 + (\frac{\gamma - 1}{2}) M_\infty^2 ((\vec{\omega} \times \vec{r})^2 - \vec{V}^{\,2})\right]^{\frac{1}{\gamma - 1}} \tag{2}$$

Of course, this is not valid, in rotational regions. However, the vortical regions are thin and their fine structure has no global significance.

For the present purposes, the velocity, $\vec{V}$, is defined as the sum of an irrotational velocity field ($\vec{\nabla}\phi$) and a rotational velocity field ($\vec{q}^{\,v}$);

$$\vec{V} = \vec{\Omega} \times \vec{r} + \vec{\nabla}\phi + \vec{q}^{\,v}. \tag{3}$$

($\vec{\Omega} \times \vec{r}$ results from a rotational coordinate transformation and has no fundamental effect on the flow kinematics. It will be ignored in future discussion.) The vortical velocity, $\vec{q}^{\,v}$, will be specified to represent the trailed circulation. The use of the above velocity decomposition and the manner of defining $\vec{q}^{\,v}$ are the most unusual features of the present method and they enable us to freely convect the wake. Therefore, solving Eq. 1 amounts to a full potential solution, which is fairly standard except for the addition of a forcing function.

A lifting inviscid problem is completed by the Kutta condition, which (for a potential method) becomes a statement expressing the convection of circulation, Γ, from the trailing edge;

$$\Gamma_t + \vec{V}_{ave} \cdot \vec{\nabla}\Gamma = 0 \tag{4}$$

where $\vec{V}_{ave}$ is a local average velocity on a trailed circulation sheet and Γ equals the bound circulation of that rotor element from which a sheet element convects (this amounts to a doublet lattice representation of the wake). The present method finds the location of the trailed sheet by a Lagrangian convection of trailed circulation elements (markers). The circulation contained in these markers is then imposed on the flow as a $\vec{q}^{\,v}$ distribution. In order to find this $\vec{q}^{\,v}$, a distribution function is chosen *a priori* and then scaled such that it's integral across the wake is the required circulation,

$$\Gamma = \int \vec{q}^{\,v} \cdot \vec{dn} \tag{5}.$$

Here, $\vec{q}^{\,v}$is chosen to have a Clebsch-type of representation,

$$\vec{q}^{\,v} = \Gamma \vec{\nabla}\lambda, \tag{6}$$

that is, a strength function (the circulation) multiplied by the gradient of a normal distribution function, λ . λ is chosen to have the form

$$\begin{aligned} &\lambda(\vec{r}) = 1/2 \; sin\,(\pi S_n/2a), \; |S_n| \leq a/2 \\ &\lambda(r) = +1/2, \; S_n > +a/2 \\ &\lambda(\vec{r}) = -1/2, \; S_n < -a/2 \end{aligned} \tag{7}$$

where S_n is a (signed) normal distance from the point $\vec{r}$ to the sheet. This distribution function is defined over a distance, $'a'$, on either side of the sheet. $'a'$ is a convenient function of the local grid - typically about 4 cell intervals. Outside of this distance, λ is constant. Therefore, the effect of trailed circulation is explicitly specified in only a small

region. Note that the vortical velocities are normal to the circulation sheet - an unphysical velocity, but one which is kinematically permitted by Eqs. 1 and 3. Note also that Eq. 7 assumes that the circulation sheet has a curvature which is small compared to 'a'.

The final solution procedure is an iteration between the convection of a wake defined by trailed markers (including its' subsequent representation as a $\vec{q^v}$ field) and the solution to the potential equation.

EXPERIMENTAL AND COMPUTATIONAL MODELS

Comparisons of computed results with experimental data will be discussed. These comparisons are made for three different rotor configurations tested at IMFM and Aerospatiale. These are:

1. A 1.5m diameter, 4-bladed rotor with a rectangular planform and a linear twist of -8.3 degrees. The rotor uses a OA209 airfoil from root to tip. The significance of this rotor is that it has been the subject of several flow visualization and laser velocimetry studies (at IMFM) of its flow field - in addition to the usual performance measurements. This rotor has been referred to as "rotor 7" in various studies.

2. A 1/4 scale model of the basic Super Puma rotor. The geometry of this rotor is nearly identical to the previous rotor, except that the inboard spanwise regions use the OA213 airfoil. The outboard radii use the OA 209 and the airfoil transition region extends from .75R to .90R. Since the twist of this rotor (based on the zero-lift angle) is nearly identical to that of rotor 7, this rotor should have very similar load distribution and wake structure. The importance of this rotor is that it's size permits a much better representation of full-scale performance. This rotor is referred to as "rotor 7A".

3. A rotor identical to rotor 7A with the exception of having non-rectangular tip geometry. This rotor - referred to as "rotor 7AD" - uses a parabolic, anhedral tip, which is identical to that used on the Super Puma MK2 rotor. Fig. 5 shows a sketch of the rotor tip, which is referred to as the 'SPP8' tip. The desired effect of the anhedral is to move the tip vortex away from the blade and thereby improving its inflow distribution and performance.

In all of our computations we have used grids which range in size from 206,000 (for rotor 7) to 250,000 points (for rotors 7A and 7AD). The grids used for 7A and 7AD are nearly identical (this ensures a fair performance comparison) and are somewhat larger than the one used for rotor 7 in order to properly resolve the SPP8 tip. We have determined that the resolution of blade surface flows is a greater driver of grid density than the resolution of the wake. This is only true because of the circulation-preserving nature of the vorticity embedding method. In previous work (Ref. 15) much denser grids have been tested with no measurable improvement in accuracy and at the cost of reduced wake stability and increased CPU time. It appears, therefore, that the present grid is close to being an upper limit for an optimum size.

(Smaller grids will probably be used in future as our base of experience grows.) A typical computation with this grid involves about 10 free-wake iterations and requires about 2 hours on a Cray YMP.

RESULTS

The results, shown in this section, can be classified as follows:

1. Comparisons of wake geometry, circulation distribution, field axial velocity and performance for rotor 7 with experimental data from IMFM. Previous studies of this rotor (Ref. 15) were very useful for determining the grid types required for various rotor computations.

2. Comparisons of computed load distribution and wake geometry for rotors 7A and 7AD and the comparison of computed performance for these two rotors with Aerospatiale measurements.

Figure 6 shows the computed lift convergence for rotor 7 for various collective pitch angles. In order to start these computations an estimate of the total wake geometry is required. To obtain this estimate an artificial uniform axial flow velocity is imposed. This axial velocity defines the initial wake geometry, which is merely an undeformed spiral at the beginning of the process. At each iteration this artificial axial velocity is reduced until it is finally eliminated altogether, leaving only the wake induced velocity, which determines the geometry of the wake. Typically, this process is completed in about 4 iterations, at which time the thrust and wake geometry are fairly close to their final values. It can be seen from this figure that the thrust converges to the final value in less than 10 iterations. For some cases the solutions were continued well beyond this level with no major lift variations. It is seen in Fig. 6 that there is a tendency to predict lift values which exceed those measured. This tendency is quite general, both for the present method and for the classical integral methods as well. This overprediction probably results from the lack of appropriate structural and viscous modeling. However, these are not usually considered serious problems as long as the power/lift polars are well predicted. Therefore, a usual mode of operation for most hover performance codes is to trim the code to a specified thrust. However, we do not currently run HELIX in this mode - only the collective pitch and blade geometry are specified.

The IMFM studies of rotor 7 include measurements of the radial circulation distribution obtained from the previously described LV line-integral measurement procedure. Figure 7 shows comparisons of these circulation distributions with those obtained from the computations. It is seen that a fairly good comparison is obtained for all collectives.

Since these circulation distributions are determined by the wake, it is useful to perform direct comparisons of the computed and measured tip vortex geometry. Figures 8 and 9 show a comparison of the computed axial and radial tip vortex locations with values obtained by flow visualization at IMFM.

The comparison shown here (for rotor 7 at a collective of 10 degrees) is excellent and fairly typical. The main difference in this wake data is that the computed contraction is somewhat greater than the measured values. This ability to predict wake geometry is basic to the analysis of unconventional configurations.

In addition to comparing the computed and measured tip vortex trajectories, we have also made comparisons with measured field velocities (obtained using LV surveys). Figures 10 and 11 show comparisons of these velocities at .22 and 2.66 chords, respectively, below the flap axis of the rotor at three different azimuth angles (measured with respect to the blade quarter chord line) - again, for a collective of 10 degrees. There is a fair overall comparison of the measurements and computations for the inner 80% of the blade. The differences seen in the outer regions are greater. The main difference there is that the radial contraction (as indicated by the outboard velocity drop-off) is often greater than was indicated by the previous tip vortex comparisons. This difference may result from the assumed identification of the observed tip vortex location with the tip shed circulation centroid. It is also observed that the computations do not show the extreme velocity peaks seen in some of the measurements. Such differences easily arise from small differences in the vortex location. Further, vorticity smearing used to represent the circulation will reduce the velocity peaks unless special gridding measures are taken to resolve this region. We have not attempted such measures because vorticity embedding makes such measures unnecessary for performance applications.

We summarize our computational studies of rotor 7 with a comparison of the computed and measured performance. Power is predicted as the sum of induced power and profile power. At present, separation is not accounted for and profile power is assumed to arise only from skin friction. We further assume a turbulent boundary layer and use a simple Nash-Macdonald integral method to obtain the skin friction. This is undoubtedly an oversimplification for the low Reynolds numbers of this small model rotor. It is more common to use airfoil tables when they are available. The induced power is obtained as the integral of the normal energy flux over a volume enclosing the rotor (Ref. 16). The resulting lift/power curve is shown in Fig. 12. The measured and computed values are fairly close. However, for the above boundary layer simplifications we would expect to achieve better comparisons for larger rotors.

As mentioned earlier, similar computations have also been performed for the larger 7A and 7AD (with the SPP8 tip) rotors. Current tests of these latter two rotors do not include the extensive flow field measurements, which were obtained for rotor 7. However, since rotors 7 and 7A differ mainly in their inboard profile, it is safe to assume that the 7A flow field and circulation are very similar to that of rotor 7. Performance tests of rotors 7A and 7AD have revealed that the latter rotor has a significant Figure-of-Merit (FM)

advantage (Ref. 13). The ability to computationally emulate this improvement can be a good test for a hover performance code.

It is first required to investigate the effect of the SPP8 tip on the tip vortex trajectories. Figures 13 and 14 show the axial and radial convection of the tip vortices for these rotors operating at a collective of 10 degrees. (As expected, the vortex trajectories for rotor 7A are very close to those shown in Figures 8 and 9 for rotor 7.) The effect of the anhedral tip is clearly seen in these figures, to increase the axial convection rate prior to the first blade passage - and hence to increase the minimum distance between the rotor and the closest passing vortex. The radial contraction is also increased by the SPP8 tip and this may reduce the benefit gained by an increased axial distance from the blade. These tip trajectory changes (the increased contraction and initial axial convection) are seen for all collective pitch angles. The effect of this change in the tip vortex trajectory and blade geometry on blade circulation distribution are shown in Fig. 15. In this figure, the 7A and 7AD circulation distributions for collectives of 6 and 12 degrees are shown. They demonstrate that the computed effects of the SPP8 tip are similar for a wide range of collectives. It is seen that the major effect is a reduction in circulation near the tip. We have not yet determined the relative influence of the planform and the anhedral in producing these circulation changes.

It is important to compute the effect of the above circulation changes on the induced power. Figure 16 shows the effect of this modified circulation on the ideal figure-of-merit (a computed figure- of-merit which is based only on induced power). In order to emphasize the differences in the ideal figure-of-merit it is necessary to greatly expand the ordinate scale. On such a scale any irregularities in the computations become clear. Indeed the ideal FM (for both rotors) is best described as a narrow scatterband centered on an FM of about 0.875. Within this band there appears to be little difference between the rotors at the lower thrust values. At the higher thrust values there is more separation between the two rotors and the 7AD rotor may have an ideal FM advantage of about 0.02. In order to further pursue such induced power studies it would be necessary to refine the accuracy of the present power integration scheme. However, it does seem that the ideal FM is only a very weak function of thrust and geometry (at least for the present configurations) and it is not clear that greater induced-power accuracy will yield a significant improvement in the total performance prediction.

The total performance characteristics of these rotors is shown in Fig. 17. In this figure the computed and measured FM for rotors 7A and 7AD are shown - also on a well expanded scale to emphasize the performance differences. It is seen that for both the 7A and 7AD rotors there is a substantial difference between the computed and measured FM at the higher lift values. This difference is obviously due to a breakdown of our simple skin friction model - possibly due to stall effects. This can be remedied by obtaining

the profile power from airfoil tables (assuming that there is no appreciable tip separation) or a local Navier-Stokes solution. However, the comparison between measured and computed figure-of-merit is excellent at the lower thrust values. A more important feature of this comparison is the fact that the incremental differences in performance are well predicted. In view of the above discussion it is clear that much of the performance gains of the 7AD rotor are due to profile power improvements. It also appears that the present accuracy of the method is adequate for many performance computations - both of an absolute and a comparative nature. This capability implies a considerable potential for the present method as an analysis and design tool.

CONCLUDING REMARKS

In many respects, HELIX-I is a standard full-potential CFD rotor code. This implies an ability to efficiently predict the detailed flow on a rotor blade - including three-dimensional, transonic and weak viscous effects (with the use of appropriate boundary-layer analyses). However, the code is unique in that it uses the Clebsch kinematical flow description to specify a freely convecting wake. The resulting code is the first full-potential CFD code with the ability to model free wake convection. It is also the first CFD code of any type to predict hover performance.

We have applied this code to the study of the SPP8, anhedral, parabolic tip used on the Super Puma MK2. For comparison, we also studied the rectangular-tip version of this rotor and another very similar rectangular rotor, which has been the subject of extensive flow field measurement studies at IMFM. Computations of this latter rotor have shown a very good ability to predict the tip-vortex geometry. Computed velocity fields in the wake of this IMFM rotor have compared fairly well with LV surveys. Comparisons of the computed radial circulation distributions with LV circulation line-integral values have also been good. We infer that these results are representative of the flow on the rectangular Super Puma blade, because of the similarity of the two blade geometries. Computations have shown that the SPP8 tip increases both the tip-vortex contraction and closest approach distance. This wake change together with the tip taper result in a considerable reduction in the circulation in the immediate vicinity of the tip. The changes in the inboard circulation values are relatively small. These computed changes in circulation distribution have been consistent for all collective angles. The effects of these changes on the induced power appear to be small at lower thrusts and may only be significant at higher thrust values. The total power trends and the measured performance improvement caused by the SPP8 tip are very well predicted and point to the utility of this new computational technology for practical aerodynamic hover analysis.

ACKNOWLEDGEMENTS

These computations were performed using the resources of the Numerical Aerodynamic Simulation Program (NAS) at the

NASA Ames Research Center. This work was also supported by the French Army, under contract no. 89/1433/DRET/DS/SR. We would especially like to acknowledge B.Demaret and P.Benquet for their administrative support and F.Toulmay for his assistance in the definition of the SPP8 geometry.

REFERENCES

1. R.B. Gray, "An Aerodynamic Analysis of a Single-Bladed Rotor in Hover and Low Speed Forward Flight as Determined from Smoke Studies of the Vorticity Distribution in the Wake," Princeton University *Aeronautical Engineering Department*, Report No. 356, Princeton University, Princeton, New Jersey, Sept. 1956.

2. A.J. Landgrebe, "An Analytical and Experimental Investigation of Helicopter Rotor Hover Performance and Wake Geometry Characteristics," USAAMRDL TR 71-24, June 1971.

3. F.F. Felker, T.R. Quackenbush, D.R. Bliss, and J.S. Light, "Comparisons of Predicted and Measured Rotor Performance in Hover Using a New Free-Wake Analysis," presented at the 44th Annual Forum of the American Helicopter Society, Washington,DC, June 16-18,1988.

4. J.P. Shanley, R.C Moffitt, and S.J. Davis, "Systematic correlation and Evaluation of the EHPIC Hover Analysis," Proceedings of the American Helicopter Society 46th Annual Forum, pp 1121-1134, May 1990.

5. T.R. Quackenbush, D.B. Bliss, D.A. Wachspress, and C.C. Ong, "Free Wake Analysis of Hover Performance Using a New Influence Coefficient Method," NASA CR-4150, 1988.

6. N. Kroll, "Computation of the Flow Fields of Propellers and Hovering Rotors Using Euler Equations," paper no. 28, Twelfth European Rotorcraft Forum, Garmisch-Partenkirchen, Germany, Sept. 22-25, 1986.

7. E. Kramer, J. Hertel, and S. Wagner, "Computation of Subsonic and Transonic Helicopter Helicopter Rotor Flow Using Euler Equations," paper no. 14, Thirteenth European Rotorcraft Forum, Arles, France, Sept. 8-11, 1987.

8. G.R. Srinivasan, S. Obayashi, J.D. Baeder and W.J. McCroskey, "Flowfield of a Lifting Hovering Rotor - A Navier-Stokes Simulation," Proceedings of the 16th European Rotorcraft Forum, pp 3.5.1 - 3.5.16, Vol.1, Sept. 1990.

9. K. Ramachandran, "Free Wake Analysis of Helicopter Rotor Blades in Hover Using a Finite Volume Technique," Ph.D. thesis, University of Tennessee, Knoxville, Dec. 1987.

10. J.S. Steinhoff, and K. Ramachandran, "A Vortex Embedding Method for Free Wake Analysis of Helicopter Rotor Blades in Hover," paper no. 2-11, Thirteenth European Rotorcraft Forum, Arles, France, Sept. 1987.

11. D. Favier, M. Nsi Mba, C. Barbi and C. Maresca, "A Free Wake Analysis for Hovering Rotors and Advancing Propellers," Vertica, Vol. 11, No. 3, pp. 493-511, 1987.

12. M. Nsi-Mba, "Contribution a l'etude experimentale et numerique de l'aerodynamique d'une voilure tournante. Cas d'un rotor d'helicoptere en vol stationnaire," These no. 207.208.89.46, thesis for Docteur es Sciences Mathematiques, l'Institut de Mecanique des Fluides de Marseille, Universite d'Aix Marseille II, 26 September, 1989.

13. A.Vuillet, M.Allongue, J.J.Philippe, and A.Desopper, "Performance and Aerodynamic Development of Super Puma MK II Main Rotor with New SPP8 Blade tip Design," Proceedings of the 15th European Rotocraft Forum, Paper No. 35, Amsterdam, Sept 12-15, 1989.

14. M.Allongue and J.P.Drevet, "New Rotor Test Rig in the Large Modern Wind Tunnel," Proceedings of the 15th European Rotocraft Forum, Paper No. 98, Amsterdam, Sept 12-15, 1989.

15. M.Nsi Mba, K.Ramachandran and F.X. Caradonna, "Experimental and Computational Studies of Hovering Rotor Flows," Paper No. 30, Presented at the 3rd International AHS Technical Specialist Meeting on Rotorcraft Basic Research, Atlanta, Ga, March 25-27.

16. K. Ramachandran, C. Tung and F.X. Caradonna, "Rotor Hover Performance Prediction Using a Free Wake, CFD Method," Journal of Aircraft, Vol. 26, No. 12, pp 1105-1110, Dec 1989.

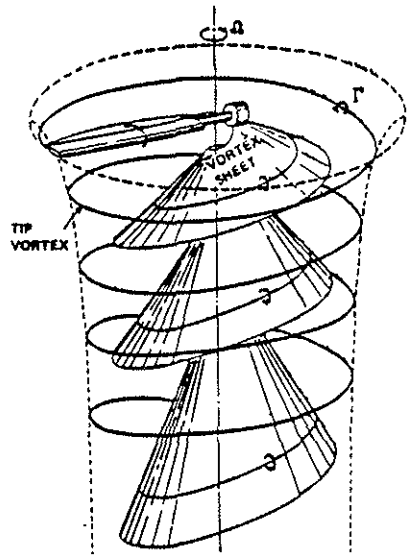

Figure 1: A schematic of the wake of a hovering rotor (from Ref. 1).

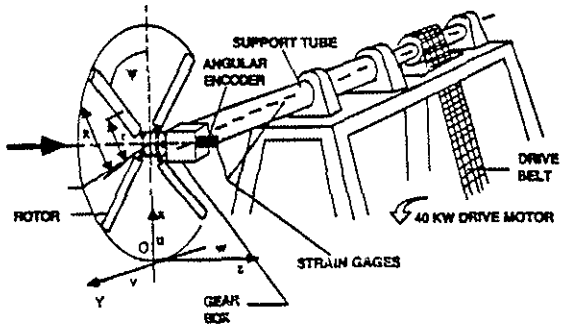

Figure 2: A schematic of the stand used for operating rotors in the IMFM wind-tunnel.

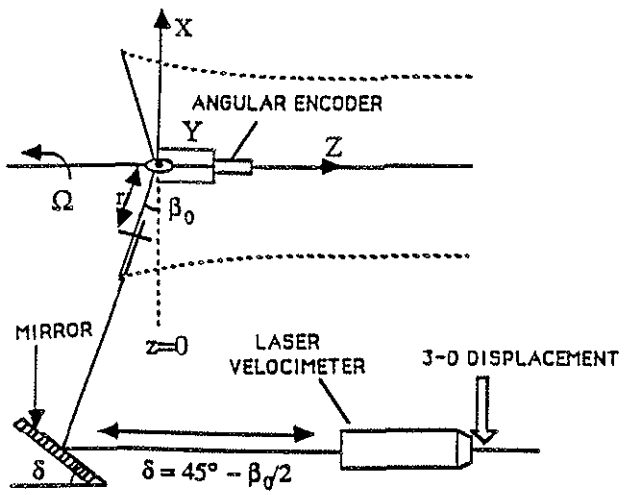

Figure 3: A schematic of the laser velocimetry set-up used for obtaining rotor wake and circulation integral data.

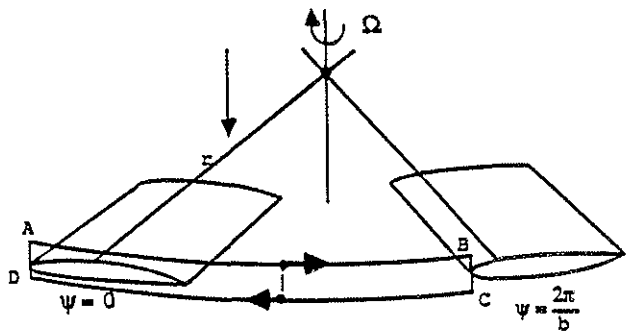

Figure 4: Integration path used for obtaining the present radial circulation distributions.

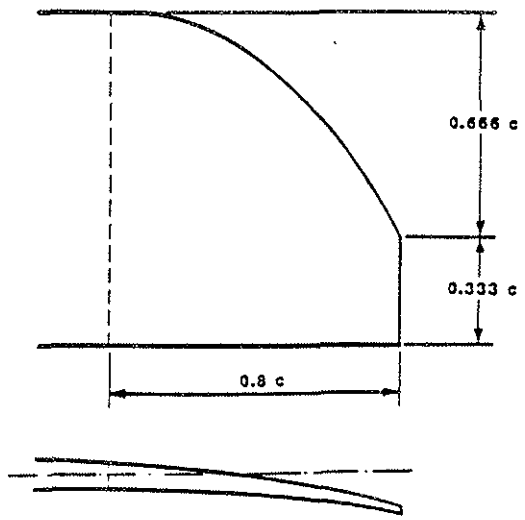

Figure 5: The SPP8 tip shape.

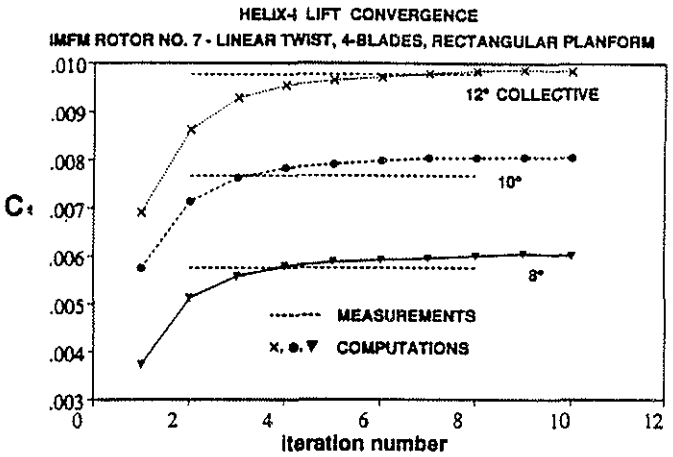

Figure 6: Computed thrust convergence histories for a hovering rotor operating at various collectives.

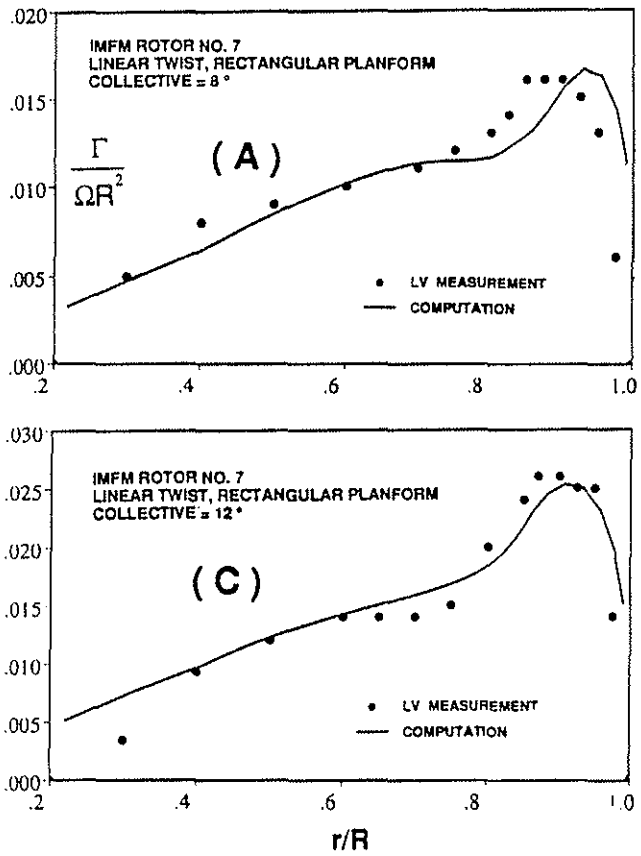

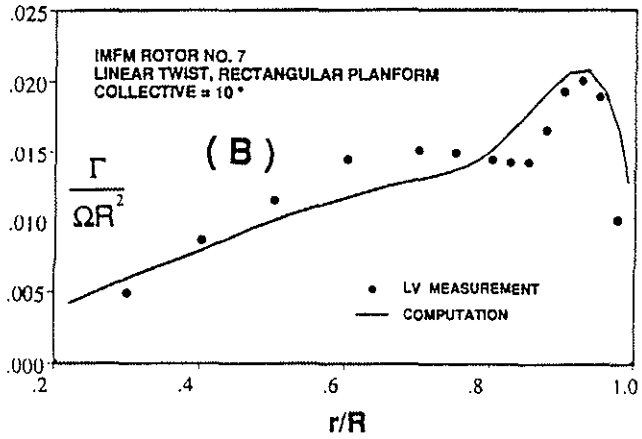

Figure 7: A comparison of measured and computed circulation distributions for rotor 7.

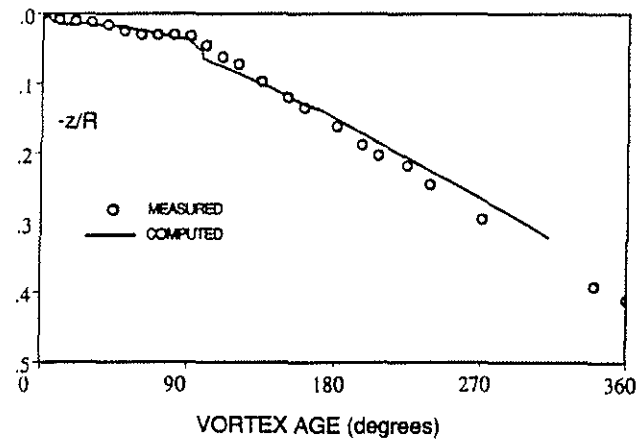

Figure 8: A comparison of the measured and computed tip-vortex axial convection for rotor 7 operating at 10° collective.

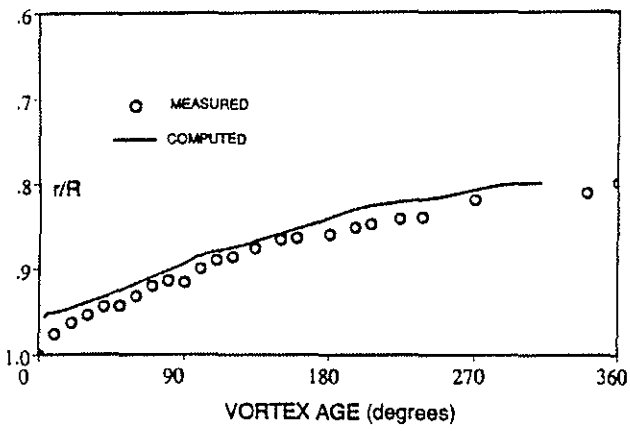

Figure 9: A comparison of the measured and computed tip-vortex radial convection for rotor 7 operating at 10° collective.

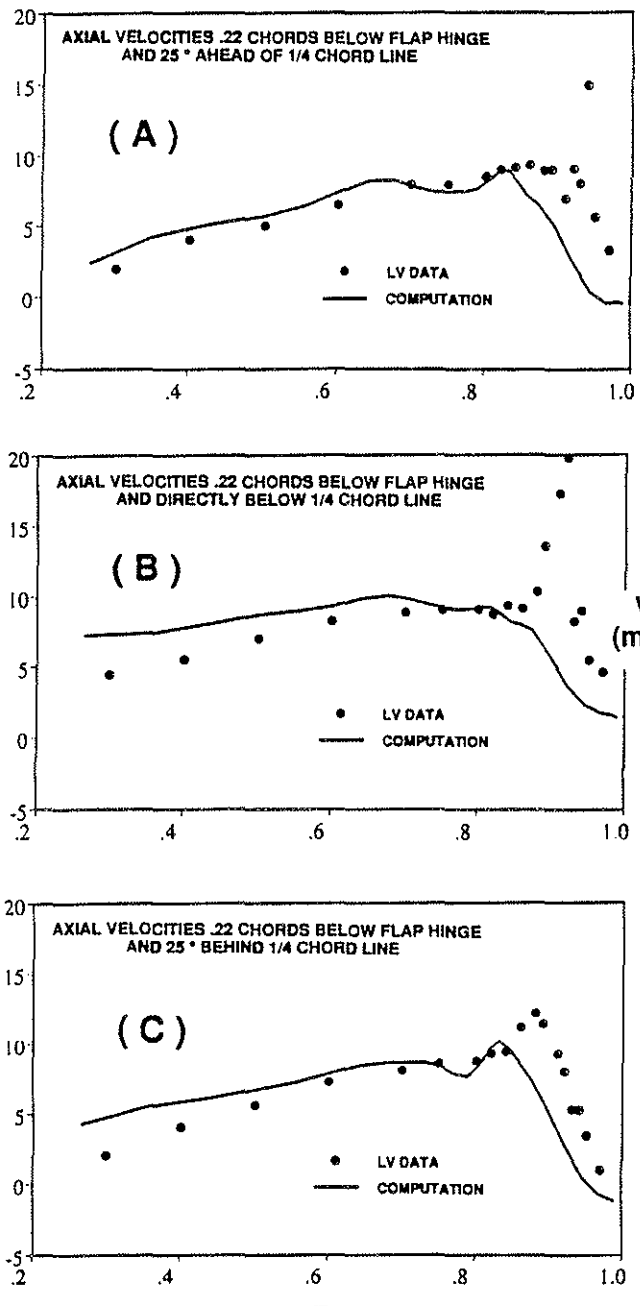

Figure 10: Computed and measured axial velocities on a plane located at 0.22 chords below the rotor flap hinge axis. Rotor 7 operating at 10° collective.

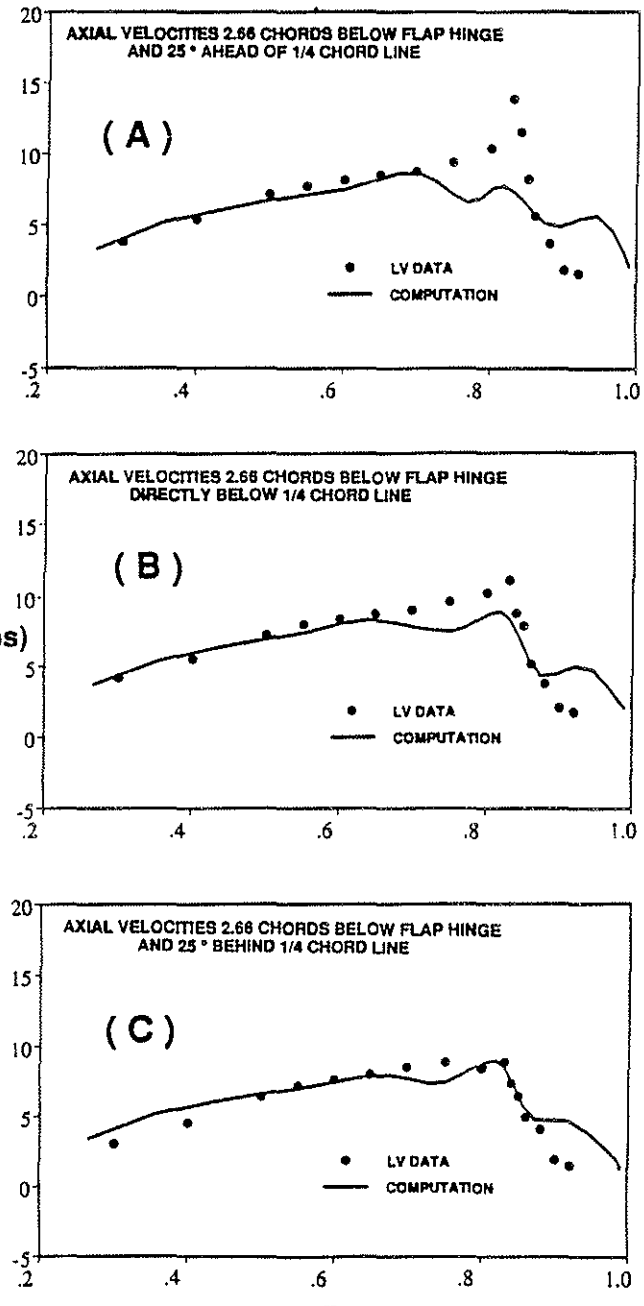

Figure 11: Computed and measured axial velocities on a plane located at 2.66 chords below the rotor flap hinge axis. Rotor 7 operating at 10° collective.

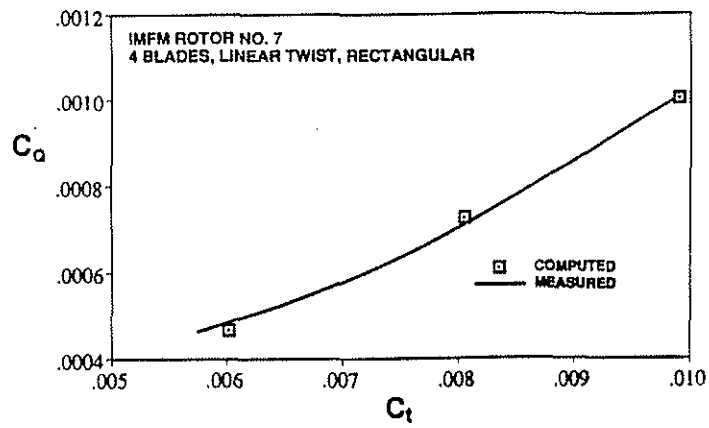

Figure 12: The measured and computed thrust/power polar of rotor 7.

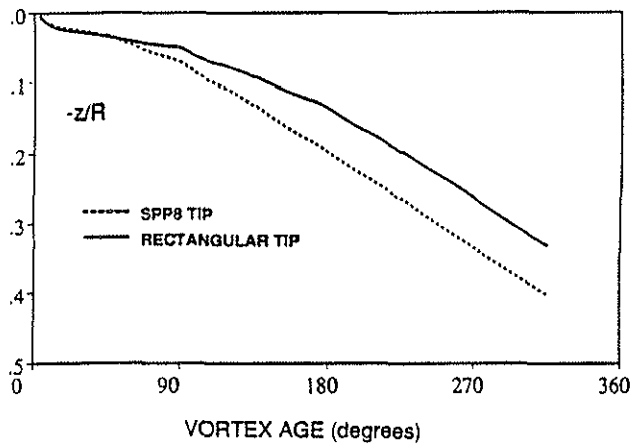

Figure 13: The effect of tip shape on the tip-vortex axial convection. A comparison of a rectangular and a parabolic, anhedral tip. Rotors operating at 10° collective.

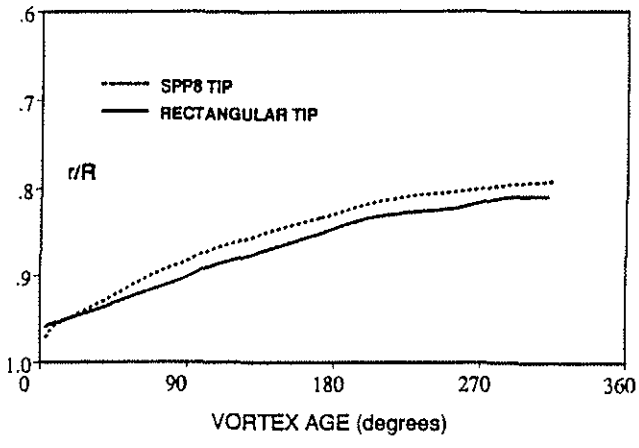

Figure 14: The effect of tip shape on the tip-vortex radial convection. A comparison of a rectangular and a parabolic, anhedral tip. Rotors operating at 10° collective.

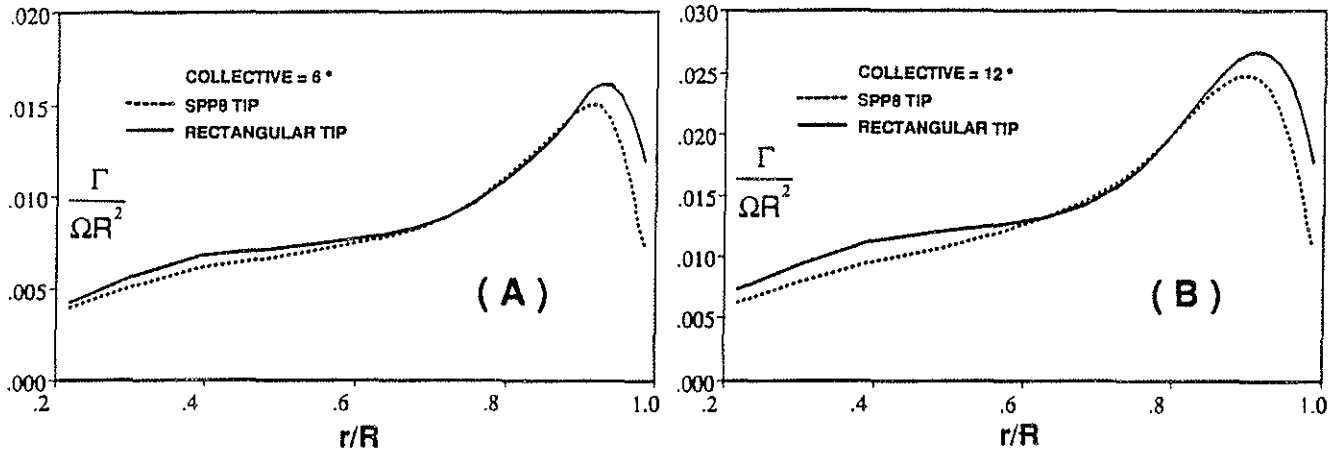

Figure 15: The effect of tip shape on the radial circulation distribution of hovering rotors. A comparison of a rectangular and a parabolic, anhedral tip.

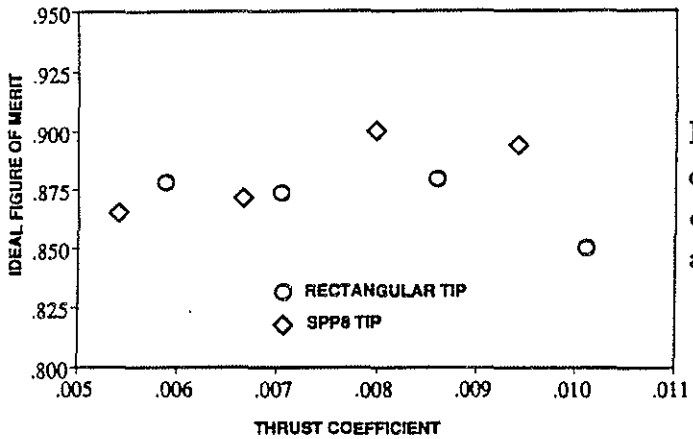

Figure 16: The computed effect of tip shape on the induced power of hovering rotors. A comparison of a rectangular and a parabolic, anhedral tip rotor.

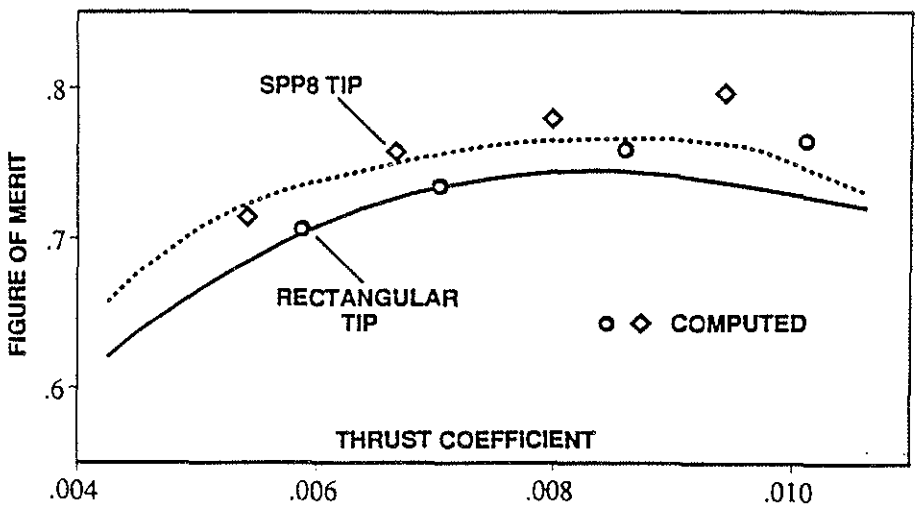

Figure 17: The effect of tip shape on the performance of hovering rotors. A comparison of measured and computed (using HELIX-I) figure-of-merit.